

# The quantitative analysis of tungsten ore using X-ray microCT: Case study



Stephan G. Le Roux<sup>a</sup>, Anton Du Plessis<sup>a,\*</sup>, Abraham Rozendaal<sup>b</sup>

<sup>a</sup> CT Scanner Facility, Stellenbosch University, Stellenbosch, South Africa

<sup>b</sup> Earth Science Department, Stellenbosch University, Stellenbosch, South Africa

## ARTICLE INFO

### Article history:

Received 1 June 2015

Received in revised form

8 September 2015

Accepted 9 September 2015

Available online 14 September 2015

### Keywords:

Ore minerals

X-ray tomography

Tungsten/scheelite

## ABSTRACT

Volumetric quantification of ore minerals is of interest using non-destructive laboratory X-ray tomography, as it allows high throughput, fast analysis, without any/limited sample preparation. This means traditional chemical analysis can still be performed on the same samples, but good information can be provided in a very short time assisting in exploration, mining and beneficiation decision making as well as sample selection for further chemical analysis. This paper describes a case study in which tungsten WO<sub>3</sub>/scheelite is quantified in 35 mm diameter drill core samples and compared to subsequent traditional chemical analysis for the same samples. The results show a good correlation and indicates that laboratory X-ray CT scanning could replace the more time consuming traditional analytical methods for ore grading purposes in some types of deposits. Different image processing methods are compared for these samples, including an advanced thresholding operation which reduces operator input error. The method should work equally well for other types of ore minerals in which the mineral of interest is the most dense particle in the scan volume, and for which the bulk of the particle sizes are at least 3 times larger than the scan resolution.

© 2015 Elsevier Ltd. All rights reserved.

## 1. Introduction

X-ray microCT (XCT) has increasingly been used in the geological and earth sciences in the last few decades (Cnudde and Boone, 2013; Mees et al., 2013). There are a variety of different applications in which the method is used with great success, including visualization and quantification of soil macro-porosity formed through chemical displacement (Perret et al., 1999) quantifying and characterizing the different types of porosity in reservoir rocks (Van Geet et al., 2000), petroleum engineering by imaging the distribution of porosity and permeability of fluid phases in porous rocks (Akin and Kavscek, 2003), development of new software for mineral characterization in geological samples (Ketcham and Carlson, 2001) and determining the liberation efficiency of copper using through heap leaching (Miller et al., 2003) and phosphate rock flotation techniques (Miller et al., 2009), amongst others.

To date, there have been limited reports of the use of XCT to determine ore grade or concentration. In a study by Godel (Godel, 2013) XCT scans were performed on Cu–Ni–PGE samples in order to determine the different mineral phases, shapes and as well as

quantify each of the mineral phases in the sample (Godel, 2013). Some research has also been performed to investigate mineral size and shape relating to the origin of a Fe–Ti–(V) oxide deposit in China (Liu et al., 2014).

The industry standard techniques for determining ore grade are X-ray Fluorescence (XRF), Inductively Coupled Plasma Spectroscopy atomic emission (ICP-OES) and Inductively Coupled Plasma Mass Spectroscopy (ICP-MS) analysis on powder milled samples to determine bulk major and trace element concentrations. These are destructive techniques which are not only time consuming but require significant sample preparation and result in the loss of information with regard to particle/grain sizes and particle distribution in the sample. The advantage XCT has over these techniques is that it is non-destructive, requires no sample preparation if the sample dimensions are within the required range and can be used to perform a fast analysis of the mineral phases in situ. Recent studies have used XCT in conjunction with non-destructive XRF, however this was only applied to small samples and can only do surface analysis and does not take the entire sample into account (Boone et al., 2011; Cnudde et al., 2013).

To date some attempts have been made to quantify ore minerals using XCT with limited success. A very recent study (Lin et al., 2015) investigated the accuracy and reproducibility of volumetric quantification, and showed how this is affected by different sources of error, using an ore sample. In their work a global

\* Corresponding author. Tel: +27 21 808 9389.

E-mail address: [anton2@sun.ac.za](mailto:anton2@sun.ac.za) (A. Du Plessis).

threshold is applied and the voxels in the selected region are counted. An improvement to this method is the use of a surface determination around the edges of ore minerals, allowing sub-voxel accuracy through the use of a 3D surface determination algorithm. Sub-voxel accuracy is realized with a local thresholding algorithm as has been demonstrated on different types of samples by (Reinhart et al., 2010; Becker et al., 2012). Additionally, the human error in threshold choice as demonstrated in Lin et al. (2015) can be overcome to a certain degree by a semi-automated thresholding operation. Both of the above improvements are demonstrated in this case study.

The purpose of this case-study paper is to demonstrate the method for fast XCT analysis to quantify ore mineral content and ore grade and to demonstrate how a reduction in user input error can be made during segmentation. In this case study scheelite-rich core samples obtained from the Riviera tungsten–molybdenum deposit (Rozendaal and Scheepers, 1995) are analyzed. The results from the XCT scans are directly correlated with subsequent analysis of the same samples by an industry-standard destructive technique: in this case Sodium Peroxide Fusion ICP.

## 2. Materials and methods

Individual XCT scans were performed on four 35 mm-diameter scheelite bearing drill core samples. The samples were scanned at the Stellenbosch University CT Scanner Facility using a General Electric Phoenix V|Tome|x L240/NF180 at 50  $\mu\text{m}$  resolution, 500 ms image acquisition time at 200 kV, 100  $\mu\text{A}$  and the X-ray beam was filtered with 1.5 mm Cu. Reconstructions were performed with system-supplied Datos reconstruction software, based on a modified Feldkamp algorithm, and incorporated a beam hardening correction factor. The reconstructed data volumes were analyzed using Volume Graphics VGStudio Max 2.2 using a 16 bit data type. Powder X-ray Diffraction (XRD) was performed at iThemba labs with a BRUKER AXS with a D8 Advance diffractometer and measurement of  $\theta$ – $\theta$  scan in locked coupled mode. After initial XCT analysis was completed, the drill core samples were sent for Sodium Fusion ICP analysis at a commercial geochemical analysis services company SGS Minerals Services Pty Ltd.

In the first step of the 3D data analysis, the entire core sample is selected using a region growing tool and the air surrounding the

sample is removed. The histogram of the core sample now consist of only two peaks, it is assumed that the left peak represents the bulk silicate mineral matrix and the right peak the much denser tungsten minerals (Fig. 1). In the schematic (Fig. 1), the tungsten mineral and silicate matrix is separated by a vertical segmentation line. This illustrates a typical global thresholding operation in which all material to the right of the vertical line is selected to create a region of interest, from which volumetric measurements can be made and further analysis can be performed.

However due to the overlap of the peaks at the base of the histogram, the region of interest contains some greyscale values linked to the silicate matrix as well as missing some of the greyscale values linked to the tungsten mineral as illustrated by the dotted lines in (Fig. 1). This initial region of interest is selected through an automated global segmentation function in the software which detects the two dominant peaks and places a global segmentation line on the average gray value in the dip between the peaks. At this stage an advanced surface fit is performed on the region of interest which uses this automated global segmentation line as a starting point (Fig. 1). Next a local threshold gradient search is performed in the vicinity of the global threshold, effectively detecting the sharpest change in gray value at the region boundary.

Not only can the 3D local surface determination create sub-voxel accurate boundaries from which volumes can be determined, but the human error can be limited by the use of a local gradient search within a pre-determined range. An example of this is demonstrated on a tungsten particle in Fig. 2 in a slice image, whereby the outer yellow line is the initial threshold selection, the perpendicular lines on this contour indicates the local gradient search distance and the new surface determination resulting from this process is shown in brighter yellow (inner contour). In this case a thin channel is now exposed which would have falsely added to the volume of tungsten.

This method allows for sub-voxel accuracy in the detection of the boundary of the mineral grain, effectively taking into account partial volume affects and to some extent attenuation artefacts to determine a very accurate grain boundary and in the process limits user error. Clearly this method is also superior to thresholding along (square) voxel boundaries. This new surface created on each of the grains represents only the tungsten minerals and excludes the silicate matrix surrounding the grains. A new region of interest is now created for the tungsten grains from this surface

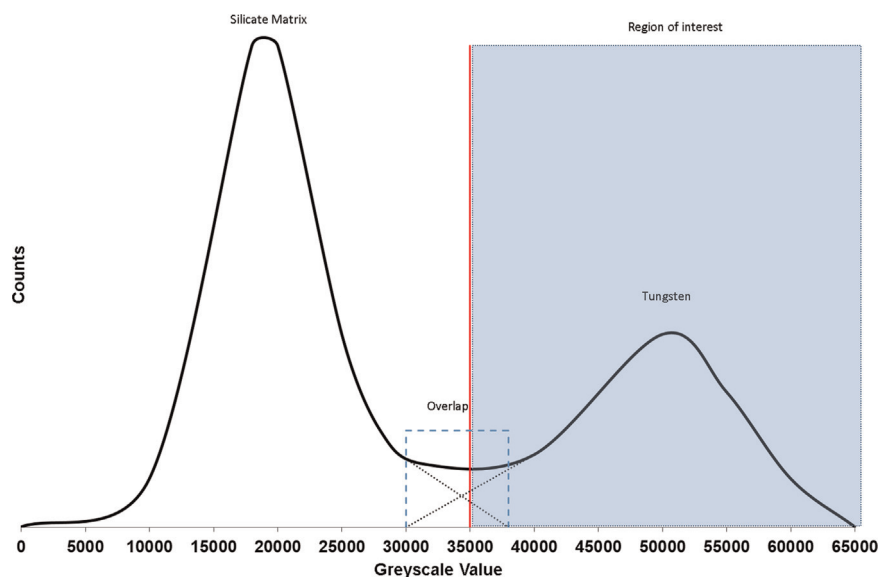
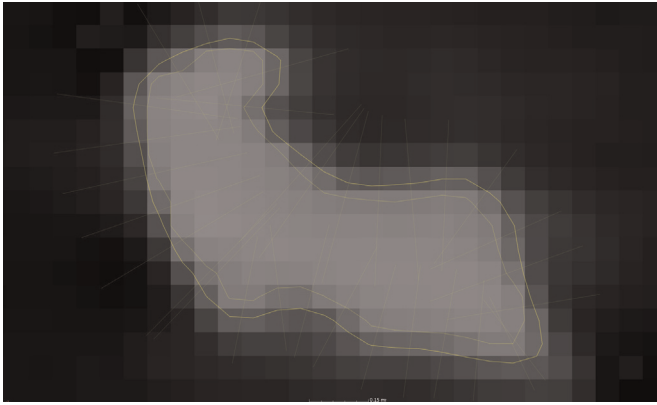


Fig. 1. Schematic of the initial segmentation used to select the bulk of the greyscale values associated with the tungsten minerals.



**Fig. 2.** The line with perpendicular search lines indicates the region of interest determined by the segmentation indicated in Fig. 1, while the new solid line without short perpendicular lines indicates the result of an advanced refinement from this surface. This improved local surface determination allows more accurate edge boundary determination. (For interpretation of the references to color in this figure, the reader is referred to the web version of this article.)

determination and is used to determine the volume of the grains, and can be used for further grain size distribution analysis or visualization.

### 3. Results

In this study the segmentation method described above was applied to four tungsten-bearing samples from the Riviera deposit (Rozendaal and Scheepers, 1995). In order to perform the analysis it is assumed that the tungsten minerals are the densest particles in the sample and have a substantial enough histogram peak which can be used for a reasonable initial threshold choice in the analysis, which was the case in these samples. It is therefore envisaged that the method is not applicable to low-grade ores. Fig. 3 illustrates a 3D view of a XCT scan performed on drill core W01 with a particle size analysis performed on the mineral grains. The color-coding is based on tungsten grain volume, i.e. the largest

grain is red and the smallest blue. The image to the left shows the core surface while the image to the right is a semi-transparent 3D view showing the location of the grains in the core in 3D.

During the analysis the segmentation line for each of the samples (W01–W04) was placed at the bottom dip of the histogram between the two dominant peaks (Fig. 4).

From this segmentation the volume of the mineral particles of each of the core samples are calculated using the method described in the previous section. Each of the core samples are weighed in order to calculate the grade per weight percent (Table 1).

The weight of scheelite in each core is calculated by multiplying the segmented and XCT-calculated mineral volumes (from Fig. 4) by the density of scheelite ( $6.1 \text{ g/cm}^3$ ). By performing a simple weight ratio calculation between the total weight of the core sample and the weight of the scheelite minerals an average grade can be deduced as shown in Table 1.

### 4. Discussion

In this study it is assumed that the second peak of the bi-modal histogram contains only tungsten and that no other dense minerals are present in the core samples (Fig. 4). In order to justify this assumption, samples were sent for powder XRD analysis to determine the mineral phases present in the sample. The powder XRD results indicate that the core samples mainly consists of scheelite, pyrite, pyrrhotite and quartz as shown in Fig. 5. However this does not indicate that scheelite is necessarily the densest mineral in the core samples. The calculated theoretical X-ray attenuation coefficient (Berger et al., 1998) of each of these minerals is plotted in Fig. 6 to determine which of these minerals attenuate the most X-rays indicating which mineral will appear the densest in the XCT data.

The combined results of the XRD (Fig. 5) and theoretical X-ray attenuation (Fig. 6) indicate that scheelite is the only tungsten mineral and is the most X-ray dense mineral in the core samples.

To date various thresholding algorithms have been used for segmentation e.g., global threshold and voxel counting (Lin et al.,

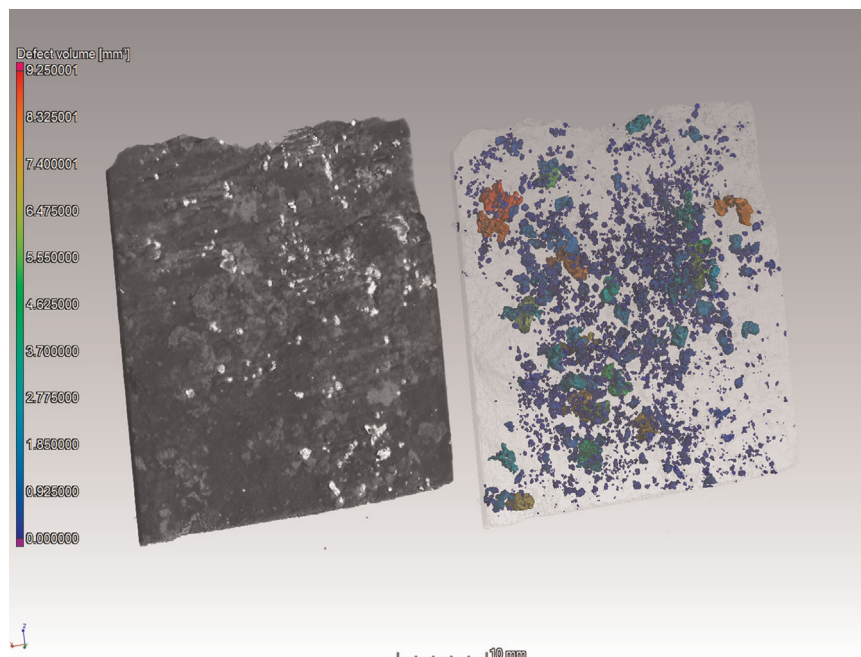


**Fig. 3.** CT scan image of drill core W03, showing a color coded scheelite mineral grain analysis, with largest volume grains in red and smallest in blue (scan at  $50 \mu\text{m}$  voxel resolution). (For interpretation of the references to color in this figure legend, the reader is referred to the web version of this article.)

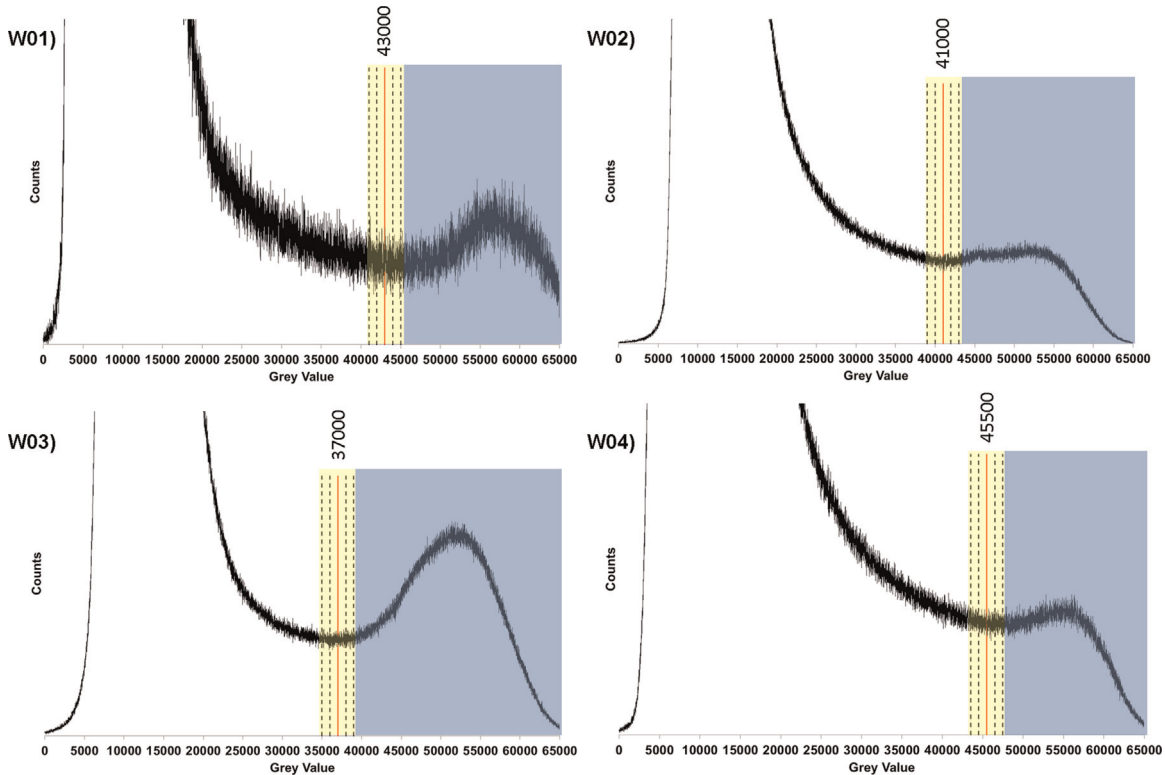


**Fig. 4.** Histogram of each core sample W01–W04 indicating the ideal global threshold (red line). The yellow region indicates selections that vary the volumetric result in a range of up to 10%, when using a simple global threshold only. However with the advanced method this variation is less than 3%. (For interpretation of the references to color in this figure legend, the reader is referred to the web version of this article.)

**Table 1**

Grade calculation of the four core samples using the advanced segmentation method.

Sample	Core weight (g)	CT (W) volume(mm <sup>3</sup> )	CT (W) grade(wt%)
W01	77.00	39.26	0.20
W02	55.40	214.37	1.51
W03	63.00	375.37	2.32
W04	40.00	149.30	1.45

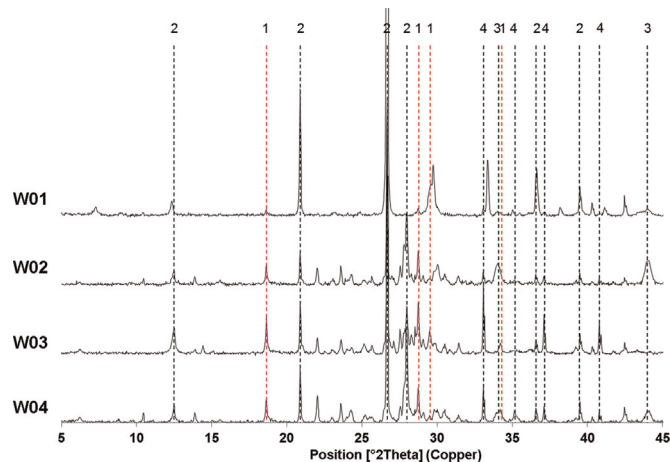


**Fig. 5.** Powder XRD analysis of all four core samples demonstrating that scheelite is the only tungsten mineral and is the most dense mineral are present in the various cores. (1) Sheelite; (2) Quartz; (3) Pyrite; (4) Pyrrhotite.

2015), maximum entropy algorithm (Kapur et al., 1985) and dual thresholding (Vlassenbroeck et al., 2007), however these methods have their limitations and in most cases are based on visual

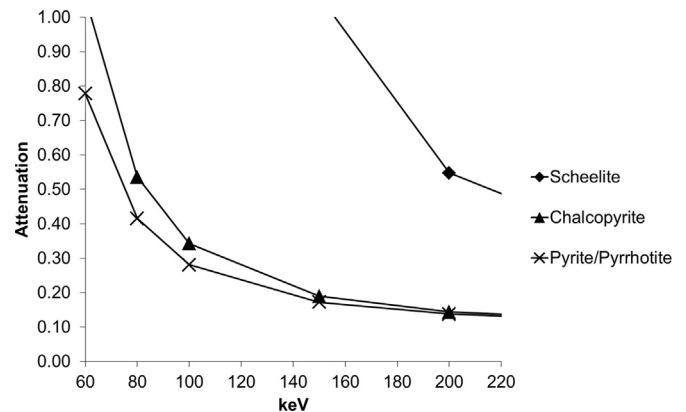


**Fig. 6.** Theoretical X-ray attenuation coefficient of the range of dense minerals that are present in the core samples. The graphs indicate that at energies between 60 and 200 keV, scheelite will have the highest attenuation by a large margin.

inspection of the material transition (material edge). When using a global threshold method, voxel counting is also limited in its accuracy especially for small particles as shown by Lin et al. (2015) and the number of voxels inside a small object can vary depending on the cubic voxel's orientation relative to the object, i.e. different scan angles can affect the result.

In order to demonstrate the effectiveness of the advanced segmentation method, it is compared to global threshold segmentation (Fig. 7). In this comparison global threshold values from 13,000 to 63,000 are selected in intervals of 1000. The volume determination for varying threshold choices is calculated using both methods to illustrate the variance of the result with threshold choice. Both methods can be directly compared and clearly the advanced method allows a larger range of threshold choices with minimal effect on the result (Fig. 7). The maximum percentage

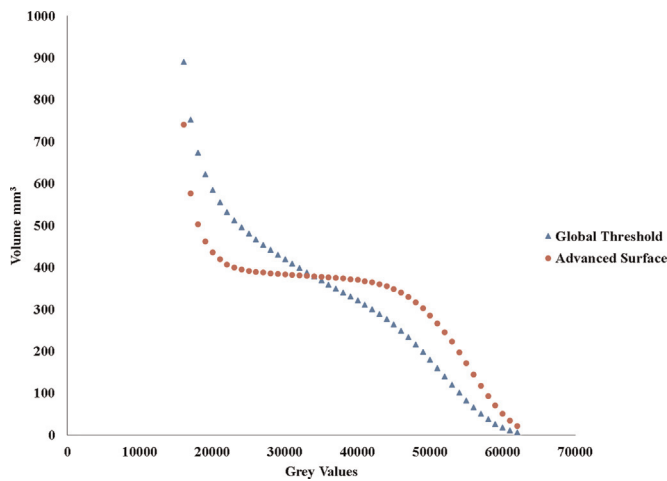


**Fig. 7.** A comparison between the tungsten volumes calculated using both Global and Advanced threshold methods. The volumes of the Global threshold indicate a strong variation: as the greyscale value is increased the volume of the selected region decreases. The advanced segmentation has a range of values in the middle that produce almost the same volume.

difference of the calculated volume left and right of the intersection (gray value 26,000–42,000) between the Global Surface (SG) and the Advanced Surface (AS) (Fig. 7) is 20% and 3% respectively. It also indicates that the first 3000 gray values left and right of the intersection has a difference in calculated volume of less than 1% when using the AS method. This results in volumetric measurements that are less dependent on threshold choice and based on local greyscale gradients, hence making it more accurate.

In order to confirm the accuracy of the advanced segmentation method, the calculated tungsten grade of the four core samples were compared to industry standard Sodium Peroxide Fusion ICP (ICP) analysis (Table 1) for the exact same samples. The results indicate that the grade obtained from the Advanced Segmentation method for samples W02, W03 and W04 are well correlated to the ICP results. The XCT grade calculation of W01 however is lower than the ICP result; this could be as an error in the ICP analysis as a result of the W standards used for the ICP analysis which have a minimum concentration of 0.3 wt% (Table 2).

The results from (the two methods correlate well and what is not noted above is that the traditional method of sample submission, processing and analysis has a turnaround time of weeks to months while CT analysis can be within the same day or the same week depending on transportation and facility booking schedules. Besides ore grade information, the entire core volume is determined in the same process which can be useful for average density determination, especially useful when considering that this information is possible with much faster scans allowing higher throughput than the other analysis presented here.

In addition to the grade information provided, additional 3D information is available which is not possible by any other technique including grain size analysis, grain shape information and

**Table 2**

Expansion of the initial XCT volume analysis comparing the ICP data to the XCT data and correlation of results.

Sample	Core weight (g)	CT core volume (mm <sup>3</sup> )	CT tungsten volume (mm <sup>3</sup> )	CT tungsten grade (wt%)	ICP grade (wt%)	Difference(%)
W01	77.00	25,641	39.26	0.20	0.29	−31.52
W02	55.40	17,162	214.37	1.51	1.40	+7.65
W03	63.00	20,583	375.37	2.32	2.20	+5.49
W04	40.00	13,113	149.30	1.45	1.40	+3.85

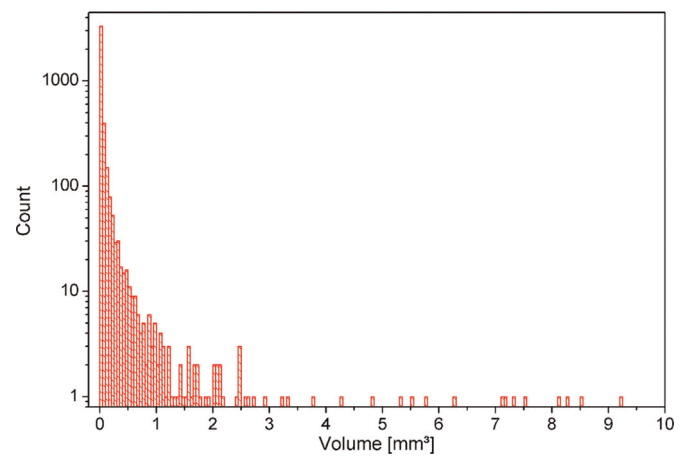


**Fig. 8.** Particle size distribution of the quantified scheelite particles in the W03 sample. The particle size distribution indicates large quantities of small particles < 0.1 mm<sup>3</sup>, while the largest particle is 9.24 mm<sup>3</sup> with an effective diameter of 5.63 mm.

3D distribution of mineral grains in the core. Fig. 8 shows the grain size distribution indicating a large number of small grains < 1 mm<sup>3</sup> in volume.

The CT method quantifies the entire core, but is limited to the resolution capability which is limited by the field of view of the system. This determines the smallest quantifiable features or grains, which is generally limited to comprise at least 8 voxels. This results in a spherical feature of diameter 0.1 mm in this case study as the minimum-diameter detectable particle (due to the voxel resolution 0.05 mm and assuming a spherical feature will cover 2 × 2 × 2 voxels). Hence all particles with diameter less than 0.1 mm will suffer from partial volume effects and not be included in the analysis. In this type of deposit, this is acceptable and is known beforehand. The resulting particle size distribution of mineral grains in situ can thus be provided from the determined surface data, with results shown in Fig. 8. The histogram indicates that the largest particles are in the 10 mm<sup>3</sup> range, while the average particle size is 0.089 mm<sup>3</sup> (equivalent diameter=0.554 mm). The largest particle in this core sample is 5.63 mm in diameter, and there are 4246 particles larger than 0.1 mm in this core, more parameters for all four core samples are indicated in Table 3.

The type of scan produced here can be done in 1 h for inspection only and with 1 additional hour for analysis as described in this paper. Since there are a range of CT service providers, the method is accessible and cost effective. In addition to ore grading and grain analysis in situ, the method can be used to make a selection of samples for further analysis, based on 3D visual and grade information.

## 5. Conclusion

An advanced segmentation method is demonstrated to quantify the ore grade of 35 mm diameter drill core samples using

**Table 3**

Tungsten mineral grain analysis.

	Largest grain volumes (mm <sup>3</sup> )	Avg grain size (mm)	Effective grain diameter(mm)
W01	1.08	0.039	2.31
W02	8.98	0.025	4.59
W03	9.24	0.089	6.61
W04	3.51	0.015	3.44

laboratory XCT. A scan of a drill core section allows volumetric ore determination when the ore mineral is the densest mineral in the sample, and when there are no overlapping densities of other minerals. Additional information can be gained by a variety of tools (such as XRF, XRD, ICPMS as shown in this case study) as well as from geological knowledge of the samples. This case study demonstrates that quantitative results from semi-automated analysis is consistent with traditional analysis such as ICP. From these results it is clear that XCT can confidently be used as a tool to quantify the grade of drill core samples, as well as provide additional 3D grain information such as grain sizes, number of grains and 3D distribution of grains.

## References

- Akin, S., Kovscek, A.R., 2003. Computed Tomography in Petroleum Engineering Research. 215. Geological Society, London, pp. 23–38. <http://dx.doi.org/10.1144/GSL.SP.2003.215.01.03>, Special Publications.
- Becker, B., Maier, D., Reinhart, C., 2012. Computer tomography has arrived in automated inspection processes, combining material and geometry analyses. In: Proceedings the 18th World Conference on Non-Destructive Testing. April, pp. 16–20.
- Berger, M.J., Hubbell, J.H., Seltzer, S.M., Chang, J., Coursey, J.S., Sukumar, R., Zucker, D.S., Olsen, K., 1998. XCOM: photon cross sections database. NIST Standard Reference Database 8 (XGAM).
- Boone, M., Dewanckele, J., Cnudde, V., Silversmit, G., Van Ranst, E., Jacobs, P., Van Hoorebeke, L., Vincze, L., 2011. 3D phase separation and identification in granite. *Geosphere* 7 (1), 79–86.
- Cnudde, V., Boone, M.N., 2013. High-resolution X-ray computed tomography in geosciences: a review of the current technology and applications. *Earth-Sci. Rev.* 123, 1–17. <http://dx.doi.org/10.1016/j.earscirev.2013.04.003>.
- Cnudde, V., De Boever, W., Dewanckele, J., De Kock, T., Boone, M., Boone, M., Silversmit, G., Vincze, L., Van Ranst, E., Derluyn, H., Peetermans, S., Hovind, J., Modregger, P., Stampanoni, M., De Buysser, K., De Schutter, G., 2013. Multi-disciplinary characterization and monitoring of sandstone (Kandla Grey) under different external conditions. *Q. J. Eng. Geol. Hydrogeol.* 46 (1), 95–106.
- Godel, B., 2013. High-resolution X-ray computed tomography and its application to ore deposits: from data acquisition to quantitative three-dimensional measurements with case studies from Ni–Cu–PGE deposits. *Econ. Geol.* 108 (8), 2005–2019. <http://dx.doi.org/10.2113/econgeo.108.8.2005>.
- Kapur, J.N., Sahoo, P.K., Wong, A.K.C., 1985. A new method for gray-level picture thresholding using the entropy of the histogram. *Comput. Vis. Graph. Image Process.* 29 (3), 273–285. [http://dx.doi.org/10.1016/0734-189X\(85\)90125-2](http://dx.doi.org/10.1016/0734-189X(85)90125-2).
- Ketcham, R.A., Carlson, W.D., 2001. Acquisition, optimization and interpretation of X-ray computed tomographic imagery: applications to the geosciences. *Comput. Geosci.* 27, 381–400.
- Lin, Q., Neethling, S.J., Dobson, K.J., Courtois, L., Lee, P.D., 2015. Quantifying and minimising systematic and random errors in X-ray micro-tomography based volume measurements. *Comput. Geosci.* 77, 1–7. <http://dx.doi.org/10.1016/j.cageo.2014.12.008>.
- Liu, P.-P., Zhou, M.-F., Chen, W.T., Boone, M., Cnudde, V., 2014. Using multiphase solid inclusions to constrain the origin of the baima Fe–Ti–(V) oxide deposit, SW China. *J. Petrol.* 55, 951–976. <http://dx.doi.org/10.1093/ptrology/egu012>.
- Mees, F., Swennen, R., Van Geet, M., Jacobs, P., 2013. Applications of X-ray Computed Tomography in the Geosciences. Geological Society, London <http://dx.doi.org/10.1144/GSL.SP.2003.215.01.01>, Special Publications.
- Miller, J.D., Lin, C.L., Garcia, C., Arias, H., 2003. Ultimate recovery in heap leaching operations as established from mineral exposure analysis by X-ray micro-tomography. *Int. J. Miner. Process.* 72 (1–4), 331–340. [http://dx.doi.org/10.1016/S0301-7516\(03\)00091-7](http://dx.doi.org/10.1016/S0301-7516(03)00091-7).
- Miller, J.D., Lin, C.L., Hupka, L., Al-Wakeel, M.I., 2009. Liberation-limited grade/recovery curves from X-ray micro CT analysis of feed material for the evaluation of separation efficiency. *Int. J. Miner. Process.* 93 (1), 48–53. <http://dx.doi.org/10.1016/j.minpro.2009.05.009>.
- Perret, J., Prasher, S.O., Kantzas, A., Langford, C., 1999. Three-dimensional quantification of macropore networks in undisturbed soil cores. *Soil Sci. Soc. Am. J.* 63 (6), 1530–1543.
- Reinhart, C., Poliwoda, C., Günther, T., 2010. How industrial computed tomography accelerates product development in the high light metal casting and inject molding industry. In: Proceedings of the 10th European Conference on Non-Destructive Testing 1.9.1.9, June 2010.
- Rozendaal, A., Scheepers, R., 1995. Magmatic and related mineral-deposits of the Pan-African Saldania belt in the Western Cape Province, South-Africa. *J. Afr. Earth Sci.* 21 (1), 107–126.
- Van Geet, M., Swennen, R., Wevers, M., 2000. Quantitative analysis of reservoir rocks by microfocus X-ray computerised tomography. *Sediment. Geol.* 132 (1–2), 25–36. [http://dx.doi.org/10.1016/S0037-0738\(99\)00127-X](http://dx.doi.org/10.1016/S0037-0738(99)00127-X).
- Vlassenbroeck, J., Dierick, M., Masschaele, B., Cnudde, V., Van Hoorebeke, L., Jacobs, P., 2007. Software tools for quantification of X-ray microtomography at the UGCT. *Nucl. Instrum. Methods Phys. Res. Sect. A Accel. Spectrometry Detect. Assoc. Equip.* 580, 442–445. <http://dx.doi.org/10.1016/j.nima.2007.05.073>.